VO 2 Substrate Effect on the Thermal Rectification of a Far-Field Radiative Diode

I y Forero-Sandoval, J A Chan-Espinoza, Jose Ordonez-Miranda, J J Alvarado-Gil, Frédéric Dumas-Bouchiat, Corinne Champeaux, K Joulain, Y Ezzahri, Jérémie Drevillon, C L Gomez-Heredia, et al.

▶ **To cite this version:**

I y Forero-Sandoval, J A Chan-Espinoza, Jose Ordonez-Miranda, J J Alvarado-Gil, Frédéric Dumas-Bouchiat, et al.. VO 2 Substrate Effect on the Thermal Rectification of a Far-Field Radiative Diode. Physical Review Applied, 2020, 14, 10.1103/physrevapplied.14.034023 . hal-03017598

HAL Id: hal-03017598
https://hal.science/hal-03017598

Submitted on 21 Nov 2020

HAL is a multi-disciplinary open access archive for the deposit and dissemination of scientific research documents, whether they are published or not. The documents may come from teaching and research institutions in France or abroad, or from public or private research centers.

L'archive ouverte pluridisciplinaire **HAL**, est destinée au dépôt et à la diffusion de documents scientifiques de niveau recherche, publiés ou non, émanant des établissements d'enseignement et de recherche français ou étrangers, des laboratoires publics ou privés.

VO_2 Substrate Effect on the Thermal Rectification of a Far-Field Radiative Diode

I.Y. Forero-Sandoval,[1,2,*] J.A. Chan-Espinoza,[2] J. Ordonez-Miranda,[1,†] J.J. Alvarado-Gil,[2]
F. Dumas-Bouchiat,[3,‡] C. Champeaux,[3] K. Joulain,[1] Y. Ezzahri,[1] J. Drevillon,[1]
C.L. Gomez-Heredia,[2] and J.A. Ramirez-Rincon[2]

[1] *Institut Pprime, CNRS, Université de Poitiers, ISAE-ENSMA, Futuroscope Chasseneuil F-86962, France*
[2] *Applied Physics Department, CINVESTAV-IPN Mérida, Mérida, Yucatán C.P. 97310, México*
[3] *Université de Limoges, CNRS, IRCER, UMR 7315, Limoges F-87000, France*

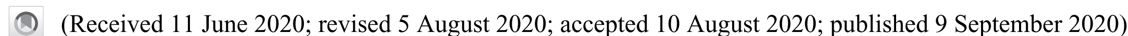

(Received 11 June 2020; revised 5 August 2020; accepted 10 August 2020; published 9 September 2020)

Thermal rectification of far-field heat currents is experimentally demonstrated by exploiting the metal-insulator transition of VO_2 driving the significant temperature variations of its emissivity, within a narrow interval of temperatures. This is achieved by measuring remarkable differences on the radiative heat flux between a VO_2 film placed in vacuum and in front of a heat fluxmeter, when their temperature difference is reversed. By testing three VO_2 films deposited on a substrate of r-sapphire, c-sapphire, and silicon, the highest rectification factor of 61% is obtained for the first film operating with a temperature difference of 40°C with respect to the fluxmeter. This rectification factor is higher than or comparable to the respective ones reported in the literature for near- or far-field radiative diodes subjected to a temperature difference of 70°C between their terminals. This experimental value is consistent with the theoretical one predicted by an analytical expression derived for the maximum rectification factor, as a function of the VO_2 emissivity in the metallic and insulating phases, sensor emissivity, and geometrical parameters. The obtained results thus show that the rectification factor of these diodes can be enhanced, while reducing the temperature difference of their terminals, by increasing not only the emissivity variations between the insulating and metallic phases of VO_2 films deposited on r-sapphire, but also decreasing their emissivity in the metallic phase.

DOI: 10.1103/PhysRevApplied.14.034023

I. INTRODUCTION

The control of heat currents by means of thermal diodes [1–5], thermal transistors [6–10], thermal logical gates [11,12], and even thermal memories [13,14] has recently attracted significant interest due to its potential applications for processing information with heat. In particular, these thermal diodes are capable of rectifying heat currents when the temperature difference between their two terminals are reversed [15,16]. An ideal thermal diode would allow passing heat in one (forward) direction and block it in the opposite (backward) one. In general, the thermal performance of a thermal diode can thus be characterized by the following rectification factor normalized to unity [3,15]

$$R = \frac{||q_b| - |q_f||}{\max(|q_b|; |q_f|)}, \tag{1}$$

where q_b and q_f are the heat fluxes in the backward and forward configurations, respectively. Among the different thermal diodes of conductive [17–20], convective [21,22], and radiative [23,24] heat currents that were proposed, the latter ones generally exhibit higher rectification factors. Furthermore, theoretical models showed that near-field radiative diodes usually yield better thermal rectifications than far-field ones [10,25], due to the significant contribution of surface phonon polaritons involved in the near-field regime [26,27].

Theoretical [3] and experimental [28,29] studies have shown that the metal-insulator transition (MIT) of vanadium dioxide (VO_2) can efficiently be used to make up thermal diodes. This reversible phase transition occurs at around 68°C [30,31] and induces significant changes of the thermal [29,32,33], electrical [34,35], and optical [28,30,34–36] properties of VO_2. By using terminals of Si and VO_2 (350-nm-thick film grown on c-sapphire) separated by an approximately 140-nm vacuum gap and exchanging near-field heat with a temperature difference of 70°C, Fiorino *et al.* [23] reported a rectification factor lower than 60%. In the far-field regime, on the other hand, Ito *et al.* [24] found a maximum rectification factor of 66% by using terminals of fused quartz and VO_2 (deposited on a silicon substrate) separated by 1 mm and operating with a

*iyforeos@gmail.com
†jose.ordonez@cnrs.pprime.fr
‡frederic.dumas-bouchiat@unilim.fr

 © 2020 American Physical Society

temperature difference of 70°C. These experimental works [23,24] indicate that far-field thermal diodes are not only easier to implement in practice than near-field ones, but also they could yield higher rectification factors, provided that a suitable VO_2 terminal is used.

In this work, three VO_2 films deposited on substrates of *r*-sapphire, *c*-sapphire, and silicon are tested as one of the terminals of a far-field thermal diode to experimentally assess its rectification factor. The highest rectification factor of 61% is obtained with *r*-sapphire and a temperature difference of 40°C between the diode terminals. Even though this optimal rectification factor is comparable to the ones reported in the literature [23,24], it represents an improvement to them, as it is obtained with a reduction of 30°C on the temperature difference of the diode terminals. This significant reduction is the result of the relatively narrow temperature interval spanning the phase transition of the VO_2 and *r*-sapphire sample and its implementation is expected to lower the energy required to generate the rectification effect and hence facilitate the operation of radiative thermal diodes. Furthermore, an analytical expression for the maximum rectification factor is also derived, as a function of the VO_2 emissivity in the metallic and insulating phases, sensor emissivity, and geometrical parameters.

II. EXPERIMENTAL SETUP

Our thermal diode consists of a VO_2 film at temperature T_{VO_2} exchanging heat by far-field radiation with a heat-flux sensor (HFS) at temperature T_s, as shown in Fig. 1(a). Taking into account that the temperature variations of the emissivity ϵ_{VO_2} of VO_2 are driven by its MIT appearing at the critical temperature T_c, the temperature interval $(T_{VO_2}; T_s)$ has to contains T_c for capitalizing on the MIT of VO_2. Therefore, in the forward configuration, the heat flux (q_f) flows from the VO_2 film to the HFS $(T_{VO_2} > T_s)$ and its value is driven by the relatively low emissivity $[\epsilon_{VO_2(m)}]$ of VO_2 in its metallic phase. In the backward configuration defined by the interchange of the temperature values $(T_{VO_2} < T_s)$ [15,16], on the other hand, the heat flux (q_b) exhibits an opposite direction and is enhanced $(q_b > q_f)$ by the emissivity $[\epsilon_{VO_2(i)} > \epsilon_{VO_2(m)}]$ of VO_2 in its insulating phase. The average emissivity ϵ_s of the HFS is considered to be independent of temperature and is determined from the FTIR spectra for wavelengths from 8 to 15 μm through the Perkin Elmer Spectrometer (Model Frontier NIR-MED) [36].

The VO_2 film is deposited on a substrate ($VO_2 + S$) and separated from the HFS by a vacuum gap of 2.3 mm to radiatively couple them in the far-field regime [37], as shown in Fig. 1(b). The lateral dimensions of the VO_2 films and HFS are $A_{VO_2} = 1.5 \times 1.5$ cm^2, $A_s = 1 \times 1$ cm^2, respectively; and their temperatures are controlled with Peltier cells (TED) and Proportional -Integral -Derivative (PID) controllers (Tetech, TC-48-20) attached to them. The temperatures are measured by means of thermistors of 0.9 mm in diameter (Tetech, MP-2444), placed as shown in Fig. 1(b). The cold face of each Peltier cell is chilled by a flux of water at a mean temperature T_w. The whole system is placed in a vacuum chamber evacuated with a pressure below 10^{-5} Torr to suppress the conductive heat currents through the intracavity air to values smaller than 0.1% of the blackbody radiation. The linear response of the HFS to heat-flux variations depends on its average

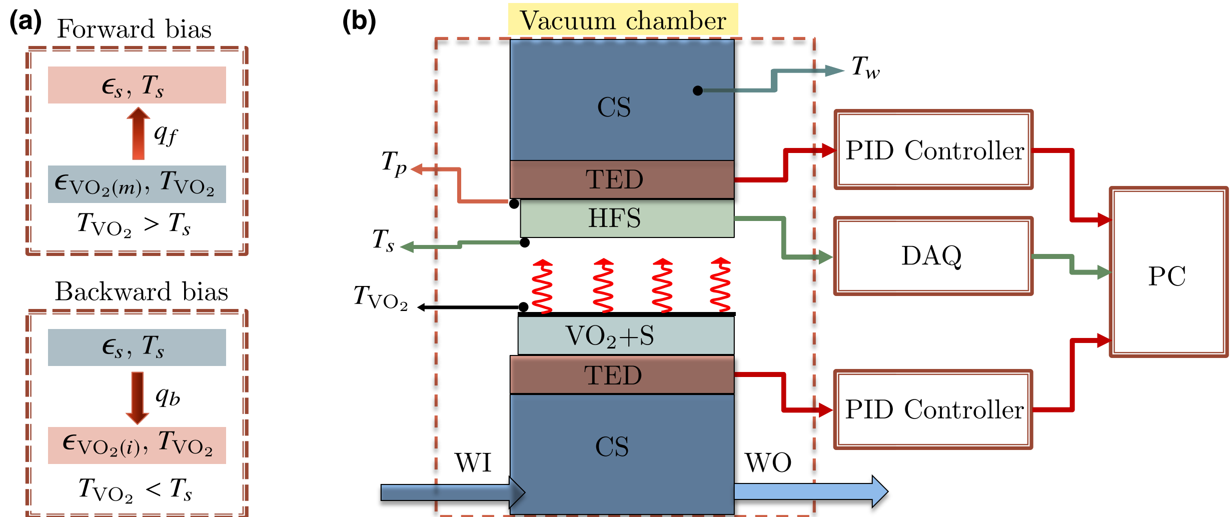

FIG. 1. Schemes of the (a) forward and backward configurations of the considered radiative thermal diode along with (b) its experimental setup. The direction of the radiative heat flux q_f (q_b) is determined by the temperature condition $T_{VO_2} > T_s$ $(T_{VO_2} < T_s)$. HFS, heat-flux sensor; $VO_2 + S$, VO_2 + substrate; TED, Peltier cell; CS, cooling system; WI, water inlet; WO, water outlet; DAQ, data-acquisition system; T_w, water temperature; T_p, Peltier temperature; T_s, HFS temperature; T_{VO_2}, VO_2 temperature.

temperature $T_a = (T_p + T_s)/2$ and the conversion from voltage to heat flux is determined by means of the calibration curve provided by the HFS manufacturer (greenTEG, gSKIN®XP). Data acquisition (DAQ) is performed by means of a Keysight USB system (U2300A).

A. Temperature control

Figure 2(a) shows the ability of our experimental system to maintain, increase or decrease the temperature of each terminal, when the set-point temperature T_{set}, controlled by a PID and represented by the red line, is modified. Initially, the system is taken to a steady state with $T_{\text{VO}_2} = T_s = 40\,^\circ\text{C}$, by fixing $T_{\text{set}} = 40\,^\circ\text{C}$ in both terminals. Next, T_{VO_2} is increased by means of the new set point $T_{\text{set}} = 45\,^\circ\text{C}$, which is reached by the VO_2 film after a few minutes. This process is repeated in steps of $5\,^\circ\text{C}$ up to $T_{\text{VO}_2} = 80\,^\circ\text{C}$ (black line). Finally, the VO_2 film is cooled down by repeating this procedure from 80 to $40\,^\circ\text{C}$ (black line). The temperature oscillations around the set points are smaller than $0.1\,^\circ\text{C}$, which shows that the system response to the increase or decrease of the temperature of both terminals is smooth enough to ensure that T_{VO_2} and T_s are well defined for accurately measuring the exchanged heat flux under steady-state conditions. In addition, the experimental data for the heat flux are recorded about 2 min after reaching the steady state and, therefore, the heat-flux values are independent of the heating and cooling speeds and time, as the typical response time of VO_2 to a change of temperature is of a few milliseconds [38]. When fast heating rates are explored, large oscillations around the set point are observed before stabilization and there is no way to determine if the heat-flux values correspond to a heating or cooling process. On the other hand, during the whole experiment, the water temperature T_w (purple line) raises around $1.6\,^\circ\text{C}$, as a result of the work done by the water pump and the extraction of heat from the Peltier cells.

Figure 2(b) shows the typical heat flux q as a function of time, for a VO_2 film deposited on c-sapphire. q is determined by means of $q = V/s$, where $V\,(\mu\text{V})$ is the measured voltage and $s[\mu\text{V}/(\text{Wm}^{-2})]$ is a temperature-dependent factor given by $s = 21.03 + (T_a - 22.5) \times 0.0254$, as provided by the sensor manufacturer. The average heat flux thus obtained is $132.477 \pm 0.047\ \text{Wm}^{-2}$, which is then used to determine the rectification factor of the thermal diode under consideration.

B. Calibration

The measured heat flux q as a function of temperature T_{VO_2} is shown in Fig. 3(a) for the heating-cooling cycle of a VO_2 and c-sapphire sample between 30 and 90°C. Note that during both the heating and cooling processes, q varies almost linearly with T_{VO_2}, for low and high enough values of T_{VO_2}, as it typically occurs for materials with temperature-independent emissivities. By contrast, for intermediate temperatures between 62 and 68 °C (64 and 58 °C), the heating (cooling) curve exhibits a significant drop (rise) of 118% (105%) due to the insulator-to-metal (metal-to-insulator) transition of the VO_2 terminal. The temperature shift between the heating and cooling curves is partially due to the intrinsic thermal hysteresis of VO_2, as reported in the literature [28]. During the whole cycle, the value of T_w increases $1.9\,^\circ\text{C}$, but it does not affect the sensor temperature T_s [Fig. 3(b)], due to the use of a PID controller.

Note that even though the heat flux is driven by the MIT of VO_2, its value does not reduce to zero for $T_{\text{VO}_2} = T_s = 30\,^\circ\text{C}$, as highlighted by the rectangle in Fig. 3(a). This indicates the presence of an nonradiative contribution detected by the HFS. This extra heat flux q_c is attributed to the heat conduction between the HFS and water, and,

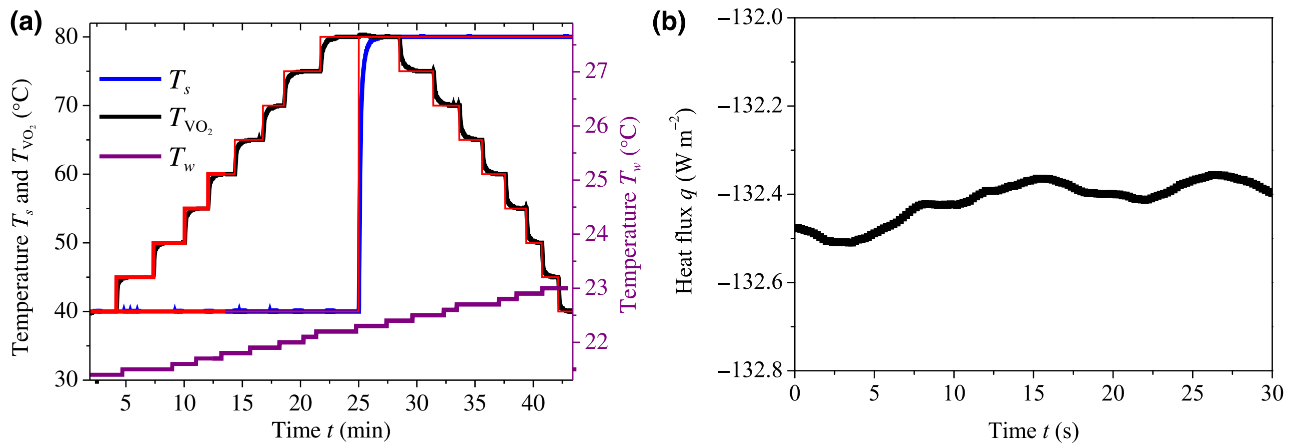

FIG. 2. Typical time evolution of the (a) temperature of the diode terminals (T_{VO_2}; T_s) and water T_w along with the (b) heat flux q recorded for a VO_2 film deposited on c-sapphire. Measurements in (b) are done for $T_s = 70\,^\circ\text{C}$ and $T_{\text{VO}_2} = 30\,^\circ\text{C}$.

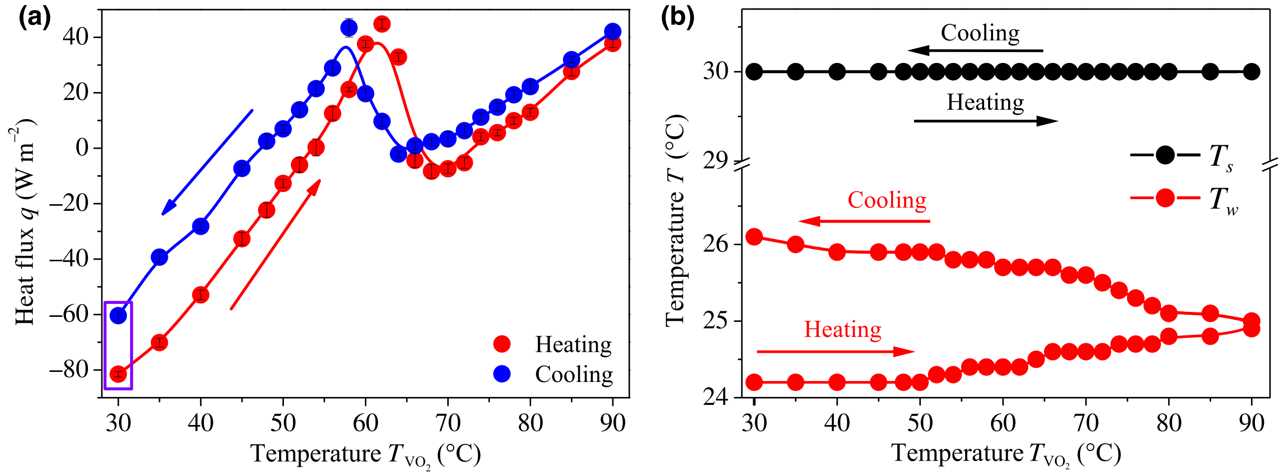

FIG. 3. (a) Heat flux and (b) temperatures T_s and T_w as functions of the VO_2 terminal temperature, for a heating-cooling cycle between 30 and 90 °C of a VO_2 film deposited over *c*-sapphire. Each experimental data point corresponds to the average of 100 measurements. Error bars included in (a) are very small and the solid lines joining the experimental points in both (a), (b) are only guides for the eye.

therefore, it can be determined by

$$q_c = G(T_s - T_w), \qquad (2)$$

where G (Wm^{-2} K^{-1}) is an effective thermal conductance. Once the value of G is determined by using the deviation of q from zero (for $T_{VO_2} = T_s = 30\,^\circ$C), the correction to each value of q is applied by using the corresponding temperatures (T_w; T_s). This correction can be applied for all the range of temperatures covered, as can be seen in Sec. S1 within the Supplemental Material [39]. The heat-flux results thus obtained are shown in Sec. III, below.

C. Sample preparation

VO_2 films are developed by using the pulsed-laser deposition (PLD) process inside an ultrahigh-vacuum chamber (nominal pressure 5×10^{-8} mbar). An excimer nanosecond laser (LightMachinery IPEX-700, wavelength $\lambda =$ 248 nm) is focused on a pure vanadium (99.95%) metallic target under a reactive oxide atmosphere maintained at a pressure of 2200 Pa. At a determined fluence of around 3 J cm^{-2}, condensed matter is ablated and transferred to a substrate place in front of the target. Maintained at around 580 °C, the synthesized film grows on a substrate and pure phases of vanadium dioxide are obtained and crystallized, at these specific conditions.

Taking into account that the growth, microstructure, and quality of VO_2 films are strongly determined by their substrate [28], in this study, three substrates (*r*-sapphire, *c*-sapphire, and silicon) are selected to drastically modify their crystallographic orientations, grain sizes and shapes, and consequently their emissivity, as detailed in our previous work [28]. In this latter work, the temperature evolution of the emissivity of VO_2 films is measured by means of the thermal wave-resonant cavity technique, whose working principle consists in detecting periodic temperature oscillations generated by a modulated infrared laser beam heating the sample. It is thus clear that the goal and methodology of our previous article [28] are totally different than the corresponding ones of the present work developed under steady-state conditions. Due to the relatively good atomic lattice matches [40], *c*-cut and *r*-cut sapphire substrates are chosen to promote VO_2 synthesis, crystallization, orientation, and resulting properties [41,42]. The main characteristics of the three samples are summarized in Table I and their structural characterization can be seen in Sec. S2 within the Supplemental Material [39].

III. RESULTS

A. Radiative heat flux and emissivity

Figures 4(a)–4(c) show the temperature variations of the radiative heat flux q exchanged by the HFS and a VO_2 film deposited on a substrate of either *r*-sapphire or *c*-sapphire or silicon, respectively. Note that q exhibits a clear hysteresis loop, whose characteristics depend strongly on the substrate, which is in a good agreement with previous works

TABLE I. Thicknesses and area of the substrates and fabricated VO_2 films.

Sample	Thickness		Area
	VO_2 (nm)	Substrate (μm)	(cm^2)
VO_2/*r*-sapphire	300	430	2.25
VO_2/*c*-sapphire	200	500	2.25
VO_2/silicon	200	525	2.25

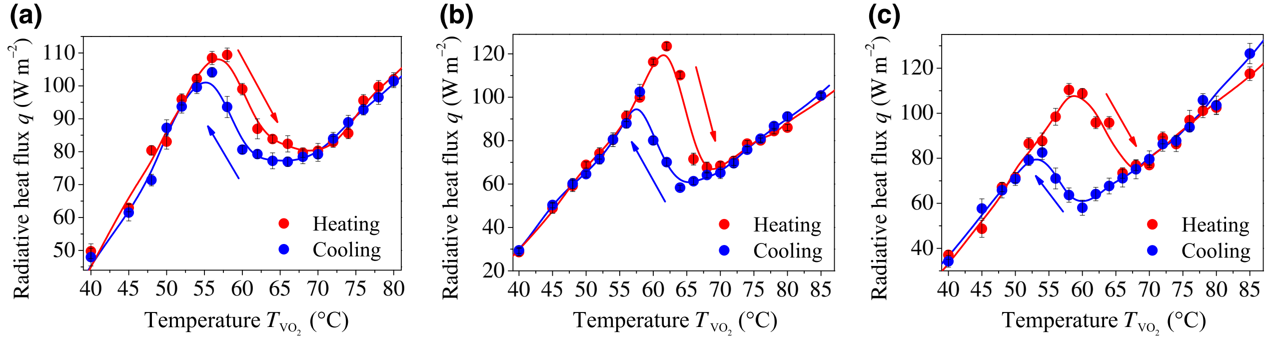

FIG. 4. Radiative heat flux as a function of T_{VO_2} for the heating-cooling cycle of a VO_2 film deposited on (a) *r*-sapphire, (b) *c*-sapphire, and (c) silicon. Red and blue experimental points stand for heating and cooling processes with $T_s = 30\,^\circ C$, respectively. Each point corresponds to the average of 100 measurements, which are used to determine the relatively small error bars. Solid lines are just guides to the eye.

[24,43,44]. Silicon yields the widest loop, while *r*-sapphire the thinnest one; and they represent the fingerprints of the MIT of VO_2. The behavior of q is driven by the emissivity and geometry of both terminals, as established by the Stefan-Boltzmann law [45]

$$q = \epsilon_{\text{eff}}\sigma(T_{VO_2}^4 - T_s^4), \tag{3}$$

where $\sigma = 5.67 \times 10^{-8}$ Wm^{-2} K^{-4} is the Stefan-Boltzmann constant and the effective emissivity $\epsilon_{\text{eff}} = \left[\left(\epsilon_{VO_2}^{-1} - 1\right)/A_{VO_2} + 1/(A_{VO_2}F) + \left(\epsilon_s^{-1} - 1\right)/A_s\right]^{-1}$, with $\epsilon_s = 0.78$ and $F = 0.36$ being the HFS emissivity and view factor [46], respectively. Details of the view-factor calculation are given in Sec. S3 within the Supplemental Material [39]. Equation (3) thus allows determining the VO_2 emissivity ϵ_{VO_2} shown in Fig. 5, by using the heat-flux values displayed in Fig. 4. One can see that the critical temperature (T_c), hysteresis width (ΔH) and slope of the heating curve (β) are different for the three VO_2 films and their values are summarized in Table II. This is reasonable, as these parameters are typically determined by the substrate [40,47–49] and the film thickness [40,48–50]. In particular, note that the samples VO_2 and silicon, and VO_2 and *c*-sapphire have hysteresis widths 4 and 1.5 times greater with that of VO_2 and *r*-sapphire, which exhibits the largest emissivity variation (0.63) between its insulating and metallic phases. The temperature evolution of the emissivities obtained for the three VO_2 films are consistent with those reported in the literature [28,51] and their values in the insulating phase are close to the corresponding ones of their substrates, as VO_2 is fairly transparent to the infrared radiation in this latter phase [34]. These results ensure that the radiative heat flux measured by our experimental setup can be considered reliable. On the other hand, note that ΔH and β have an inverse relationship, that is to say, VO_2 samples with larger hysteresis widths have slower phase transitions, in agreement with previous works [28,36,40]. These features are fundamental for the development of thermal memory devices [13,44] and thermal logic gates [11], which require large and small ΔH values, respectively.

B. Rectification factors

The radiative heat flux q measured for the forward ($T_{VO_2} > T_s = 45\,^\circ C$) and backward ($T_{VO_2} < T_s = 85\,^\circ C$) configurations between the HFS and a VO_2 film deposited

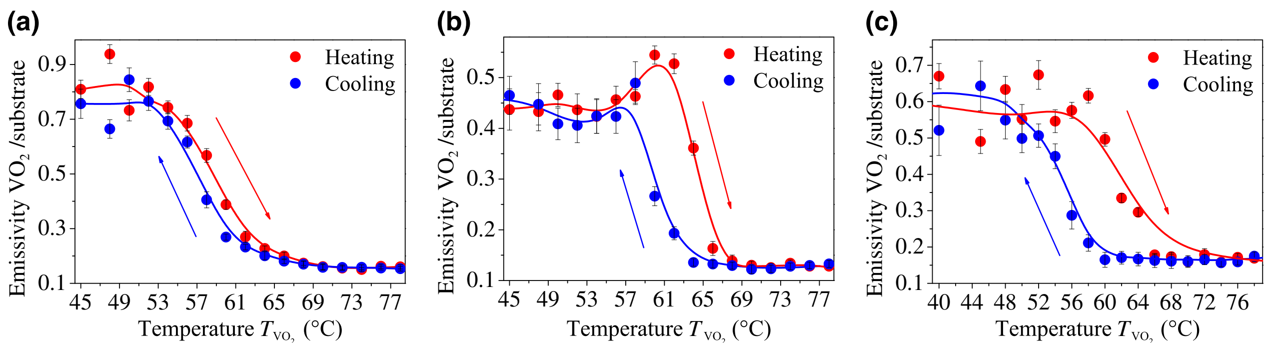

FIG. 5. Temperature evolution of the emissivity determined through Eq. (3) for a VO_2 film deposited on (a) *r*-sapphire, (b) *c*-sapphire, and (c) silicon. Solid lines represent visual guides to the eye.

TABLE II. MIT characteristics in the emissivity of VO_2 films grown on a *r*-sapphire, *c*-sapphire, and silicon substrate. Vertical arrow, for the slope β stand for the heating process.

Sample	$\Delta\epsilon_{VO_2}$	ΔH (°C)	Tc (°C)	β[°C^{-1}(↑)]
VO_2/*r*-sapphire	0.63	1.7	59	0.08
VO_2/*c*-sapphire	0.33	2.5	62	0.05
VO_2/silicon	0.43	7	60	0.03

on *r*-sapphire, *c*-sapphire, and silicon is, respectively, shown in Figs. 6(a)–6(c), as a function of the temperature difference ($\Delta T = T_{VO_2} - T_s$) between the diode terminals. The experimental data are obtained by fixing the sensor temperature $T_s = 45\,^{\circ}$C and increasing T_{VO_2} from 35 to 90 °C. Then, T_s is raised to 85 °C and T_{VO_2} decreased from 90 to 35 °C. This detailed process allowed us to clearly identify the VO_2 phase transition and any anomaly on the measured heat flux. Taking into account that the rectification factor of a thermal diode is defined in terms of the radiative heat fluxes obtained by interchanging the temperatures of the diode terminals, as established by Eq. (1), Fig. 6 displays the real operation of a thermal diode for the pair of temperatures (45;85) °C (purple points) of its terminals. This procedure is also repeated for other pairs of temperatures to determine the diode rectification factor. Note that the magnitude of q increases with $|\Delta T|$, such that its values in the backward configuration are greater than the corresponding ones in the forward bias, for a given $|\Delta T|$. This is reasonable, given that the backward configuration is driven by the VO_2 emissivity in its insulating phase, which is higher than that in the metallic one, as shown in Fig. 5. Samples grown on silicon and *c*-sapphire yield a common maximum rectification factor of 50%, which increases to 61% for the sample deposited on *r*-sapphire. This latter value surpasses the rectification factor of 56% reported by Fiorino *et al.* [23] for a near-field thermal diode based on VO_2 and operating with a temperature difference of 70 °C between its terminals. Thus, our best result not only optimizes the rectification factor, but also reduces to $85 - 45 = 40\,^{\circ}$C the temperature difference required to obtain it. This significant reduction is also present for the rectification of far-field heat currents previously reported by Ito *et al.* [24] with a similar rectification factor. In this latter work, the optimization of the rectification factor is performed by testing VO_2 and *W*-doped VO_2 films deposited on silicon, while in our present work, we do it by changing the substrate (*r*-sapphire, *c*-sapphire, and silicon) of pure VO_2 films. In addition, the methodology used by Ito *et al.* [24] is different than ours in the following aspects. (i) The HFS is placed between the VO_2 substrate and the thermoelectric device used to control the temperature and hence it can only measure conductive heat fluxes. By contrast, our HFS acts as a diode terminal and directly measures the radiative heat flux exchanged with the other diode terminal. (ii) While the calibration of our experimental setup is done with the sample to be tested, Ito *et al.* [24] performed the calibration using fused quartz and measurements with their VO_2 samples. This replacement of the material to calibrate by the one to be tested implies variations of the vacuum conditions (opening of the vacuum chamber) and the modification of the interface thermal resistance between the sample and the thermoelectric device, which could generate uncertainties on the measurements. (iii) The theoretical description of the measured heat flux is based on the fluctuational electrodynamics, whereas we apply the Stefan-Boltzmann equation that allows us to retrieve the emissivity of our VO_2 samples, as shown in Fig. 5. Even though both formalisms are correct for the considered far-field radiation, the advantage of Boltzmann approach is that it can be applied to derive an analytical expression [see Eq. (4)] for the optimal rectification factor. Based on these significant differences and the remarkable reduction of the temperature difference (from 70 to 40 °C), the present methodology and results are expected to be useful for both optimizing

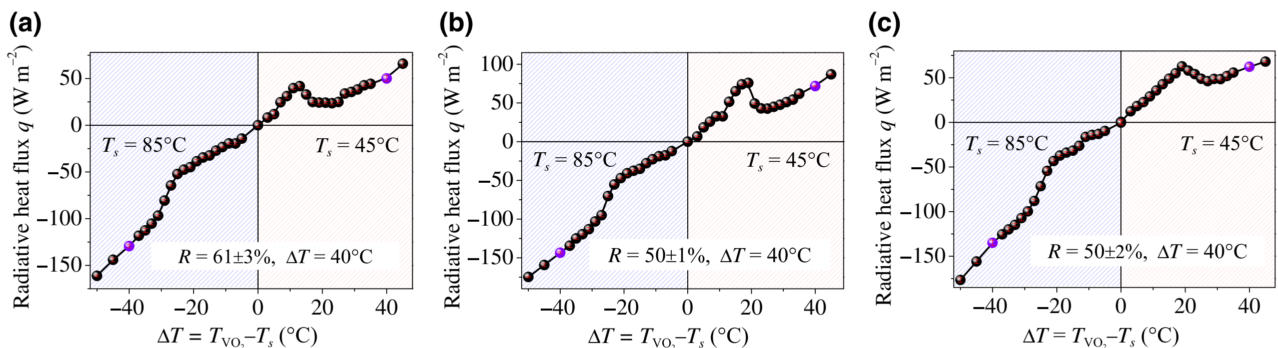

FIG. 6. Measured radiative heat flux between the HFS and a VO_2 film deposited on (a) *r*-sapphire, (b) *c*-sapphire, and (c) silicon, as a function of the temperature difference $\Delta T = T_{VO_2} - T_s$. The given rectification factors are obtained by means of Eq. (1) for $\Delta T = 40\,^{\circ}$C (q values highlighted in purple). The bluish and reddish backgrounds stand for the backward and forward configuration, respectively.

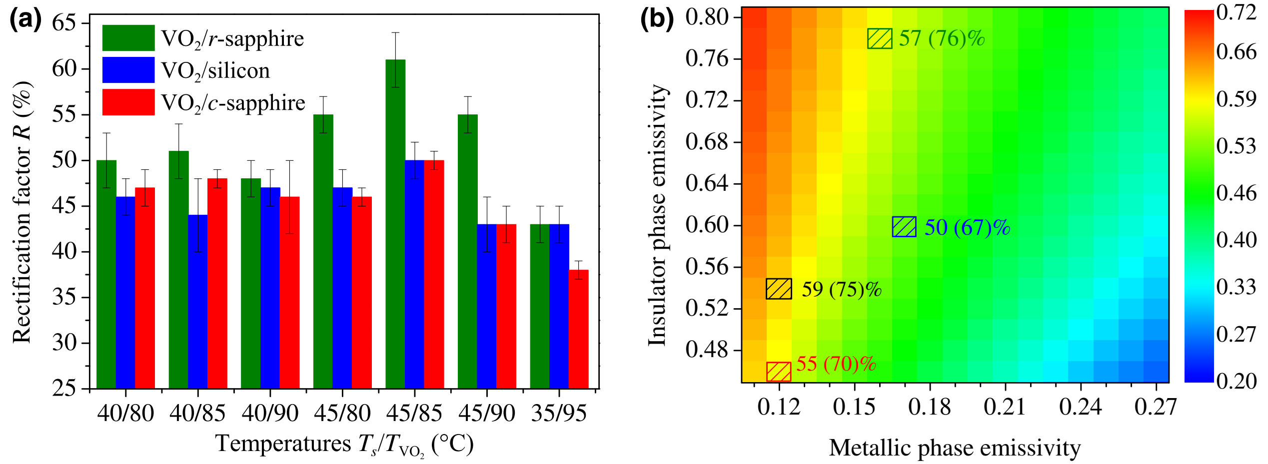

FIG. 7. (a) Summary of the rectification factors obtained by means of the experimental data shown in Fig. 6 and Eq. (1), for the three VO_2 samples and different temperature pairs (T_s; T_{VO_2}) of the diode terminals. (b) Optimal rectification factor predicted by Eq. (4) for different values of the emissivities of VO_2 in its metallic and insulating phases. The green, red, and blue squares stand for the rectification factors determined with the data reported in Fig. 5 for a VO_2 film deposited on *r*-sapphire, *c*-sapphire, and silicon, respectively. The data in parenthesis stand for an ideal thermal diode made up of two infinite parallel terminals. The black square represents the rectification factor (59%) obtained for the emissivity peak of the VO_2 and *c*-sapphire sample at 61 °C.

the rectification factor of a radiative thermal diode and reducing the temperature difference of its terminals.

Figure 7(a) shows a summary of the highest rectification factors obtained for each VO_2 sample and different temperature pair (T_s; T_{VO_2}) of the diode terminals. In order to capitalize on the VO_2 phase transition, the values of both T_s and T_{VO_2} are conveniently chosen outside it. Note that the VO_2 film grown on *r*-sapphire allows obtaining rectification factors higher than the corresponding ones yielded by the other two samples, for each temperature pair. The highest rectification is obtained for $(T_s; T_{VO_2}) = (45; 85)$°C, while the lowest one appears for $(T_s; T_{VO_2}) = (35; 95)$ °C. Taking into account that the values of these latter temperatures are well outside the VO_2 phase transition, this fact indicates that the maximum rectification factor is strongly determined by the VO_2 emissivity in its insulating [$\epsilon_{VO_2(i)}$] and metallic [$\epsilon_{VO_2(m)}$] phases. In fact, according to Eqs. (1) and (3), one can show that the optimal (maximum) rectification factor is given by

$$R_o = \frac{1 - \epsilon_{VO_2(m)}/\epsilon_{VO_2(i)}}{1 + \epsilon_{VO_2(m)}\left[A_{VO_2}(\epsilon_s^{-1} - 1)/A_s + F^{-1} - 1\right]}. \quad (4)$$

Note that R_o increases with the view factor ($F = 1$ and $A_{VO_2}/A_s = 1$ for the ideal case of infinite parallel plates), emissivity ratio $\epsilon_{VO_2(i)}/\epsilon_{VO_2(m)}$ and sensor emissivity ϵ_s, such as higher rectifications are obtained for lower emissivities $\epsilon_{VO_2(m)}$ of VO_2 in its metallic phase. Equation (4) thus establishes that the best VO_2 sample to optimize the rectification factor of a radiative diode is the one with not only the highest emissivity contrast between its insulating and metallic phases, but also with the lowest emissivity $\epsilon_{VO_2(m)}$. Among the three VO_2 samples considered in this work, both of these latter conditions are fulfilled by the VO_2 film deposited on *r*-sapphire, as shown in Fig. 5(a). The other two samples exhibit relatively large hysteresis widths, which are required for improving the performance of thermal memory devices [13,44].

Figure 7(b) shows the predictions of Eq. (4) for the emissivities in the metallic and insulator states of the three VO_2 samples displayed in Figs. 5. Optimal rectifications of 57 (76)%, 55 (70)% and 50 (67)% are obtained for the VO_2 films deposited on *r*-sapphire, *c*-sapphire, and silicon, respectively. The numbers in parenthesis stand for the rectification factors of an ideal thermal diode made up of two infinite parallel terminals. Note that even though the emissivity variation of the VO_2 and *c*-sapphire sample between its insulating and metallic phases is nearly half compared to that obtained for the VO_2/*r*-sapphire one, the optimal rectification factors determined for both samples are pretty much the same, due to the relatively low emissivity $\epsilon_{VO_2(m)}$ of the sample grown on *c*-sapphire. These results are in good agreement with the ones shown in Fig. 7(a) and reported in the literature [10,28]. The slight differences between the results displayed in Figs. 7(a) and 7(b) is attributed to the fluctuations of the VO_2 emissivity in its insulating phase, which can lead to variations of around 5% on R_o. This consistence of the optimal rectification factors obtained by means of the heat flux and emissivity values confirms that to the VO_2 film grown on *r*-sapphire is better than the other two samples to operate a radiative thermal diode. Finally, in future works, the optimal rectification factor could be enhanced by 3%, increasing the sensor emissivity from 0.78 to 0.95. In addition, we note that the emissivity peak exhibited by *c*-sapphire (at 61 °C)

could also be used to increase R_o by 3%, as shown by the black square in Fig. 7(b).

IV. CONCLUSIONS

We experimentally demonstrate the thermal rectification of far-field heat currents by exploiting the metal-insulator transition of VO_2. This is achieved by measuring the radiative heat flux between a heat-flux sensor and a VO_2 film deposited on either *r*-sapphire or *c*-sapphire or silicon. The highest rectification factor of 61% is obtained with *r*-sapphire, which is among the highest values reported in the literature with the lowest temperature difference (40 °C) between the diode terminals. This experimental value for the rectification factor is consistent with the theoretical prediction of an analytical expression that has been derived for the maximum rectification factor, as a function of the VO_2 emissivity in the metallic and insulating phases, sensor emissivity, and geometrical parameters. The obtained results thus show that the rectification factor of radiative diodes can be enhanced, while reducing the temperature difference of their terminals, by not only increasing the emissivity variation between the insulating and metallic phases of VO_2 films deposited on *r*-sapphire, but also decreasing their emissivity in the metallic phase.

ACKNOWLEDGMENTS

This work was partially supported by the projects 251882 “Investigación Científica Básica 2015”, SRE-AMEXCID-2016-1-278320, and ANR-19-CE09-0005 “EPolariton”. J.C.-E. thanks CONACYT for his master scholarship (10.13039/501100003141). The authors are grateful to J. Bante-Guerra for his technical assistance.

[1] B. Li, L. Wang, and G. Casati, Thermal Diode: Rectification of Heat Flux, Phys. Rev. Lett. **93**, 184301 (2004).

[2] C. R. Otey, W. T. Lau, and S. Fan, Thermal Rectification through Vacuum, Phys. Rev. Lett. **104**, 154301 (2010).

[3] P. Ben-Abdallah and S.-A. Biehs, Phase-change radiative thermal diode, Appl. Phys. Lett. **103**, 191907 (2013).

[4] J. Huang, Q. Li, Z. Zheng, and Y. Xuan, Thermal rectification based on thermochromic materials, Int. J. Heat Mass Transf. **67**, 575 (2013).

[5] Y. Yang, S. Basu, and L. Wang, Radiation-based near-field thermal rectification with phase transition materials, Appl. Phys. Lett. **103**, 163101 (2013).

[6] P. Ben-Abdallah and S.-A. Biehs, Near-Field Thermal Transistor, Phys. Rev. Lett. **112**, 044301 (2014).

[7] K. Joulain, J. Drevillon, Y. Ezzahri, and J. Ordonez-Miranda, Quantum Thermal Transistor, Phys. Rev. Lett. **116**, 1 (2016).

[8] J. Ordonez-Miranda, Y. Ezzahri, J. Drevillon, and K. Joulain, Transistorlike Device for Heating and Cooling Based on the Thermal Hysteresis of VO_2, Phys. Rev. Appl. **6**, 054003 (2016).

[9] H. Prod’homme, J. Ordonez-Miranda, Y. Ezzahri, J. Drevillon, and K. Joulain, Optimized thermal amplification in a radiative transistor, J. Appl. Phys. **119**, 194502 (2016).

[10] K. Joulain, Y. Ezzahri, J. Drevillon, and P. Ben-Abdallah, Modulation and amplification of radiative far field heat transfer: Towards a simple radiative thermal transistor, Appl. Phys. Lett. **106**, 133505 (2015).

[11] L. Wang and B. Li, Thermal Logic Gates: Computation with Phonons, Phys. Rev. Lett. **99**, 177208 (2007).

[12] P. Ben-Abdallah and S.-A. Biehs, Towards Boolean operations with thermal photons, Phys. Rev. B **94**, 241401 (2016).

[13] L. Wang and B. Li, Thermal Memory: A Storage of Phononic Information, Phys. Rev. Lett. **101**, 267203 (2008).

[14] V. Kubytskyi, S.-A. Biehs, and P. Ben-Abdallah, Radiative Bistability and Thermal Memory, Phys. Rev. Lett. **113**, 074301 (2014).

[15] C. Starr, The copper oxide rectifier, J. Appl. Phys. **7**, 15 (1936).

[16] E. Nefzaoui, J. Drevillon, Y. Ezzahri, and K. Joulain, Simple far-field radiative thermal rectifier using Fabry–Perot cavities based infrared selective emitters, Appl. Opt. **53**, 3479 (2014).

[17] W. Kobayashi, D. Sawaki, T. Omura, T. Katsufuji, Y. Moritomo, and I. Terasaki, Thermal rectification in the vicinity of a structural phase transition, Appl. Phys. Express **5**, 027302 (2012).

[18] E. Pallecchi, Z. Chen, G. E. Fernandes, Y. Wan, J. H. Kim, and J. Xu, A thermal diode and novel implementation in a phase-change material, Mater. Horizons **2**, 125 (2015).

[19] N. Li, J. Ren, L. Wang, G. Zhang, P. Hänggi, and B. Li, Colloquium: Phononics: Manipulating heat flow with electronic analogs and beyond, Rev. Mod. Phys. **84**, 1045 (2012).

[20] N. Roberts and D. Walker, A review of thermal rectification observations and models in solid materials, Int. J. Therm. Sci. **50**, 648 (2011).

[21] T. Villeneuve, M. Boudreau, and G. Dumas, The thermal diode and insulating potentials of a vertical stack of parallelogrammic air-filled enclosures, Int. J. Heat Mass Transf. **108**, 2060 (2017).

[22] A. Pugsley, A. Zacharopoulos, J. Deb Mondol, and M. Smyth, Theoretical and experimental analysis of a horizontal planar liquid-vapour Thermal diode (PLVTD), Int. J. Heat Mass Transf. **144**, 118660 (2019).

[23] A. Fiorino, D. Thompson, L. Zhu, R. Mittapally, S.-A. Biehs, O. Bezencenet, N. El-Bondry, S. Bansropun, P. Ben-Abdallah, E. Meyhofer, and P. Reddy, A thermal diode based on nanoscale thermal radiation, ACS Nano **12**, 5774 (2018).

[24] K. Ito, K. Nishikawa, H. Iizuka, and H. Toshiyoshi, Experimental investigation of radiative thermal rectifier using vanadium dioxide, Appl. Phys. Lett. **105**, 253503 (2014).

[25] A. Ghanekar, G. Xiao, and Y. Zheng, High contrast far-field radiative thermal diode, Sci. Rep. **7**, 6339 (2017).

[26] D. Polder and M. Van Hove, Theory of radiative heat transfer between closely spaced bodies, Phys. Rev. B **4**, 3303 (1971).

[27] P. J. van Zwol, K. Joulain, P. Ben-Abdallah, and J. Chevrier, Phonon polaritons enhance near-field thermal

transfer across the phase transition of VO_2, Phys. Rev. B **84**, 161413 (2011).

[28] C. L. Gomez-Heredia, J. A. Ramirez-Rincon, J. Ordonez-Miranda, O. Ares, J. J. Alvarado-Gil, C. Champeaux, F. Dumas-Bouchiat, Y. Ezzahri, and K. Joulain, Thermal hysteresis measurement of the VO_2 emissivity and its application in thermal rectification, Sci. Rep. **8**, 8479 (2018).

[29] G. Hamaoui, N. Horny, C. L. Gomez-Heredia, J. A. Ramirez-Rincon, J. Ordonez-Miranda, C. Champeaux, F. Dumas-Bouchiat, J. J. Alvarado-Gil, Y. Ezzahri, K. Joulain, and M. Chirtoc, Thermophysical characterisation of VO_2 thin films hysteresis and its application in thermal rectification, Sci. Rep. **9**, 8728 (2019).

[30] A. S. Barker, H. W. Verleur, and H. J. Guggenheim, Infrared Optical Properties of Vanadium Dioxide Above and Below the Transition Temperature, Phys. Rev. Lett. **17**, 1286 (1966).

[31] A. Zylbersztejn and N. F. Mott, Metal-insulator transition in vanadium dioxide, Phys. Rev. B **11**, 4383 (1975).

[32] D.-W. Oh, C. Ko, S. Ramanathan, and D. G. Cahill, Thermal conductivity and dynamic heat capacity across the metal-insulator transition in thin film VO_2, Appl. Phys. Lett. **96**, 151906 (2010).

[33] J. Ordonez-Miranda, Y. Ezzahri, K. Joulain, J. Drevillon, and J. J. Alvarado-Gil, Modeling of the electrical conductivity, thermal conductivity, and specific heat capacity of VO_2, Phys. Rev. B **98**, 075144 (2018).

[34] H. S. Choi, J. S. Ahn, J. H. Jung, T. W. Noh, and D. H. Kim, Mid-infrared properties of a VO_2 film near the metal-insulator transition, Phys. Rev. B **54**, 4621 (1996).

[35] M. M. Qazilbash, M. Brehm, G. O. Andreev, A. Frenzel, P.-C. Ho, B.-G. Chae, B.-J. Kim, S. J. Yun, H.-T. Kim, A. V. Balatsky, O. G. Shpyrko, M. B. Maple, F. Keilmann, and D. N. Basov, Infrared spectroscopy and nano-imaging of the insulator-to-metal transition in vanadium dioxide, Phys. Rev. B **79**, 075107 (2009).

[36] J. A. Ramirez-Rincon, C. L. Gomez-Heredia, A. Corvisier, J. Ordonez-Miranda, T. Girardeau, F. Paumier, C. Champeaux, F. Dumas-Bouchiat, Y. Ezzahri, K. Joulain, O. Ares, and J. J. Alvarado-Gil, Thermal hysteresis measurement of the VO_2 dielectric function for its metal-insulator transition by visible-IR ellipsometry, J. Appl. Phys. **124**, 195102 (2018).

[37] G. Wehmeyer, T. Yabuki, C. Monachon, J. Wu, and C. Dames, Thermal diodes, regulators, and switches: Physical mechanisms and potential applications, Appl. Phys. Rev. **4**, 041304 (2017).

[38] H. Wang, X. Yi, S. Chen, and X. Fu, Fabrication of vanadium oxide micro-optical switches, Sens. Actuator A Phys. **122**, 108 (2005).

[39] See Supplemental Material at http://link.aps.org/supplemental/10.1103/PhysRevApplied.14.034023 for the calibration, structural characterization, and view-factor calculation.

[40] T.-H. Yang, R. Aggarwal, A. Gupta, H. Zhou, R. J. Narayan, and J. Narayan, Semiconductor-metal transition characteristics of VO_2 thin films grown on c- and r-sapphire substrates, J. Appl. Phys. **107**, 053514 (2010).

[41] K. D. Rogers, An X-ray diffraction study of semiconductor and metallic vanadium dioxide, Powder Diffr. **8**, 240 (1993).

[42] Y. Zhao, J. Hwan Lee, Y. Zhu, M. Nazari, C. Chen, H. Wang, A. Bernussi, M. Holtz, and Z. Fan, Structural, electrical, and terahertz transmission properties of VO_2 thin films grown on c-, r-, and m-plane sapphire substrates, J. Appl. Phys. **111**, 053533 (2012).

[43] D. M. Bierman, A. Lenert, M. A. Kats, Y. Zhou, S. Zhang, M. De La Ossa, S. Ramanathan, F. Capasso, and E. N. Wang, Radiative Thermal Runaway Due to Negative-Differential Thermal Emission Across a Solid-Solid Phase Transition, Phys. Rev. Appl. **10**, 021001 (2018).

[44] K. Ito, K. Nishikawa, and H. Iizuka, Multilevel radiative thermal memory realized by the hysteretic metal-insulator transition of vanadium dioxide, Appl. Phys. Lett. **108**, 053507 (2016).

[45] B. Bird, W. Stewart, and E. Lightfoot, *Transport Phenomena* (John Wiley & Sons, New York, 2007), 2nd ed.

[46] J. R. Ehlert and T. F. Smith, View factors for perpendicular and parallel rectangular plates, J. Thermophys. Heat Transf. **7**, 173 (1993).

[47] S. Saitzek, F. Guinneton, G. Guirleo, L. Sauques, K. Aguir, and J. R. Gavarri, VO_2 thin films deposited on silicon substrates from V_2O_5 target: Limits in optical switching properties and modeling, Thin Solid Films **516**, 891 (2008).

[48] M.-W. Kim, W.-G. Jung, T.-S. Hyun-Cho, S.-J. Bae, J.-S. Chang, Jang, W.-K. Hong, and B.-J. Kim, Substrate-mediated strain effect on the role of thermal heating and electric field on metal-insulator transition in vanadium dioxide nanobeams, Sci. Rep. **5**, 10861 (2015).

[49] F. Guinneton, L. Sauques, J.-C. Valmalette, F. Cros, and J.-R. Gavarri, Optimized infrared switching properties in thermochromic vanadium dioxide thin films: Role of deposition process and microstructure, Thin Solid Films **446**, 287 (2004).

[50] R. L. Voti, M. C. Larciprete, G. Leahu, C. Sibilia, and M. Bertolotti, Optimization of thermochromic VO_2 based structures with tunable thermal emissivity, J. Appl. Phys. **112**, 034305 (2012).

[51] M. A. Kats, R. Blanchard, S. Zhang, P. Genevet, C. Ko, S. Ramanathan, and F. Capasso, Vanadium Dioxide as a Natural Disordered Metamaterial: Perfect Thermal Emission and Large Broadband Negative Differential Thermal Emittance, Phys. Rev. X **3**, 041004 (2013).